AIAA JOURNAL
Vol. 32, No. 4, April 1994

Multipoint Inverse Design of an Infinite Cascade of Airfoils

Michael S. Selig*
University of Illinois at Urbana-Champaign, Urbana, Illinois 61801

This paper describes a method for the design of an infinite cascade in incompressible flow. The method is based on conformal mapping and does allow for multipoint design. The cascade blade to be determined is divided into a desired number of segments. Over each segment, the velocity distribution is prescribed together with an inlet or outlet flow angle at which this velocity distribution is to be achieved. In this way multipoint design requirements can be met. It is necessary to satisfy several conditions that arise to guarantee compatibility with the inlet and outlet flow as well as closure of the cascade blade. Satisfaction of these conditions does not necessarily result in a cascade with all of the desired characteristics. For example, the cascade blades may be bulbous or crossed. Through Newton iteration, however, the desired characteristics may be prescribed directly. Four examples will be illustrated to demonstrate the capability of the method.

Introduction

A PRACTICAL method for the multipoint inverse design of an infinite cascade of airfoils in incompressible flow is described. The method should prove useful in the design of guidevane cascades for internal flow systems, such as wind-tunnel turning vanes. Moreover, in the design of a ducted axial flow fan, the annulus is often divided into several annular segments from hub to tip, each segment of which is designed based on the relatively two-dimensional local flow conditions. Five annular segments are usually enough to account for the considerable three-dimensional effects. The current method could be used to design each annulus. Likewise, simple compressibility corrections could be incorporated into the present method to aid in the preliminary design of axial compressor and turbine blades, albeit supercritical flow effects cannot be accounted for by such a combined method. Nevertheless, many inverse methods (two-dimensional and three-dimensional) need an initial configuration for starting their iterations. The present method could at least provide suitable initial configurations.

Of particular importance in the process of designing a new cascade (whether it be for two-dimensional or three-dimensional applications) is the ability to control the performance at more than one operating point. Most inverse cascade design methods are only capable of solving the single-point design problem; that is, the velocity distribution can only be specified for one angle of attack. Whether or not the cascade satisfies multipoint design objectives is determined through postdesign analysis at the various operating points. The current method has the explicit capability of handling multipoint design requirements from the start. As will be discussed, the cascade blade section can be divided into any number of segments along each of which, for either a given inlet or outlet angle, the velocity is tailored to correspond to a desirable aerodynamic behavior. Thus, multipoint design objectives can be satisfied during the actual design effort as opposed to designing by a single-point method and examining multipoint objectives afterwards.

It is also important to be able to control the trailing-edge angle since most turbine and many cascade blade sections have rounded trailing edges. The present method allows the designer to specify directly the desired trailing-edge angle in the range from 0 deg (a cusped trailing edge) to 180 deg (a rounded trailing edge). A rounded trailing edge raises the issue of where should the rear stagnation point be located. Although this issue is not addressed here, the ability of the present method to allow for the specification of a rounded trailing edge and also the outlet flow angle paves the way for the introduction of viscous considerations as discussed in Gostelow.[1]

A computer code (CASCADE) has been developed based on the current approach. The design method is analogous to that widely used for multipoint inverse airfoil design described in Refs. 2–5. Thus, it is expected that the current cascade design approach will have similar appeal because it allows for multipoint design and runs rapidly on a personal computer.

To place this work in a broader context, it is helpful to discuss concurrent developments in airfoil and cascade design. Mangler[6] and Lighthill[7] were the first to resolve the mathematical difficulties believed to be associated with inverse airfoil design.[8,9] These theories, which were based on conformal mapping, showed that for the inverse airfoil problem the specified velocity distribution must satisfy certain conditions. In so doing, the conformal transformation connecting the circle and airfoil plane can be found. From this transformation, the airfoil shape can be determined.

For the cascade, Lighthill[10] made a significant contribution following along similar lines. In almost analogous fashion to the isolated airfoil problem, he found that the specified velocity distribution about the cascade blade must satisfy special conditions for the mathematical problem to be well posted. Once these conditions are satisfied, the mapping can be determined to give the cascade geometry.

Advancements in airfoil design continued through improvements in numerical techniques and through the use of computers. Added to this was the multipoint design theory of Eppler (summarized in Ref. 2). Specifically, this theory made it possible to divide the airfoil into segments and specify over each segment the desired velocity distribution along with the angle of attack at which that velocity distribution is to be achieved. Consequently, conformal mapping as applied to the inverse airfoil problem remains in favor owing to the ability to solve rapidly and conveniently the multipoint design problem.[2,3]

Parallel developments in cascade design through the use of conformal mapping have not been equally successful. In fact, few recent efforts have been aimed at practical cascade design by means of conformal mapping.[11] In current use for incompressible flow are cascade design methods based on distributed singularity methods.[12–14] Such methods, however, are

Received May 23, 1992; presented as Paper 92-2650 at the AIAA 10th Applied Aerodynamics Conference, Palo Alto, CA, June 22–24, 1992; revision received Sept. 14, 1993; accepted for publication Oct. 12, 1993.

*Assistant Professor, Department of Aeronautical and Astronautical Engineering. Member AIAA.

only directly applicable to solving the single-point inverse cascade design problem. Although conformal mapping has been applied to solve the single-point design problem,[11,15-18] it is not limited to this. Conformal mapping has been employed to solve the two-point inverse design problem for which the velocity distribution is prescribed for one inlet angle on the upper surface and a different inlet angle on the lower surface.[10,19] In effect, this gives the cascade a working range. The prospect of applying conformal mapping to the multipoint inverse cascade design problem has provided the primary impetus for the work reported here.

Theory

The point of departure for inverse cascade design through the use of conformal mapping differs with respect to the inverse airfoil design problem in that for the cascade no standard transformation exists. Often, several mappings are used in sequence to take the cascade into a circle. For instance, Papailiou,[17] Garrick,[20] and Howell[21] first used a periodic mapping to take the cascade into a single closed contour in the z' plane. In this plane, points infinitely far upstream and downstream of the cascade are represented by a vortex source and vortex sink, respectively. Then, through two or more regular mappings, the contour is taken to a nearly circular contour. Finally, by Theodorsen's method or a similar procedure, this near circle is mapped via a general regular transformation into a circle about which the flow may be readily determined.

In a different approach involving only two mappings, Lighthill[10] uses first

$$e^z = z' \tag{1}$$

to map each cascade blade (spaced $2\pi i$ apart) onto a single airfoil. In this case, points infinitely far upstream ($z = x + iy \to -\infty + iy$ or simply $z \to -\infty$) are mapped to the origin, $z' = 0$, where there exists a vortex source representing the image of the inlet flow in the cascade plane. Points infinitely far downstream ($z = x + iy \to \infty + iy$ or simply $z \to \infty$) corresponding to the cascade outlet flow are mapped to infinity, $z' = \infty$. Second, the derivative of the regular mapping

$$z' = \zeta + c_0 + \frac{c_1}{\zeta} + \frac{c_2}{\zeta^2} + \cdots \tag{2}$$

is used to take the single airfoil immersed in the vortex source into a circle immersed in the vortex source.

As previous methods have demonstrated,[10,15-21] it is mathematically advantageous to isolate the singularities of the flow in the circle plane by an elementary transformation such as Eq. (1). Such an initial elementary transformation requires that one or more further mappings be employed to take the single contour into a circle. Unfortunately, for multipoint design via conformal mapping, it becomes difficult to solve the inverse problem if more than one transformation is used. In favor of solving the multipoint design problem conveniently but at the expense of involving more mathematical rigor, one transformation is used in the present method.[5,22]

General Cascade Transformation

In the current approach, a single transformation is obtained by first considering Eqs. (1) and (2). If the spacing between the cascade blades is the complex parameter l, the transformation (1) becomes

$$\exp[(2\pi i/l)z] = z' \tag{3}$$

By elimination of z' through Eq. (2), the general transformation is given by

$$\exp[(2\pi i/l)z] = \zeta + c_0 + \frac{c_1}{\zeta} + \frac{c_2}{\zeta^2} + \cdots \tag{4}$$

which takes the unit circle to the infinite cascade (Fig. 1).

As may be seen by Eq. (4), the outlet flow ($z \to \infty$) maps to infinity, and the inlet flow ($z \to -\infty$) maps to the point $\zeta = a$ according to Fig. 1 here

$$\lim_{z \to -\infty} \exp[(2\pi i/l)z] = \lim_{\zeta \to a} \left(\zeta + c_0 + \frac{c_1}{\zeta} + \frac{c_2}{\zeta^2} + \cdots\right) \tag{5}$$

or

$$0 = a + c_0 + \frac{c_1}{a} + \frac{c_2}{a^2} + \cdots \tag{6}$$

Since the velocity is to be specified, it is most convenient to work not with the mapping (4) but with its derivative. From Eq. (4), the mapping derivative can be expressed conveniently as

$$\frac{dz}{d\zeta} = \left(\frac{1}{\zeta - a}\right)\left(1 - \frac{1}{\zeta}\right)^{1-\epsilon} \exp[f(\zeta)] \tag{7}$$

where the factor $\exp[f(\zeta)]$ is a regular nonzero function for $|\zeta| > 1$ and has no zeros, poles, or discontinuities on $|\zeta| = 1$. The factor $(1 - 1/\zeta)^{1-\epsilon}$ is introduced to map the point $\zeta = 1$ to the cascade-blade trailing edge with an angle $\pi\epsilon$. The first factor is used to isolate the first-order pole.[19]

With $\zeta = re^{i\phi}$, the function $f(\zeta)$ is expressed as

$$f(\zeta) = P(r, \phi) + iQ(r, \phi) = \sum_{m=0}^{\infty} r^{-m}(a_m + ib_m)e^{-im\phi} \tag{8}$$

where $P(r, \phi)$ and $Q(r, \phi)$ are real functions, and the series converges for $r \geq 1$. On the unit circle, $r = 1$, the real and imaginary parts of $f(\zeta)$ become

$$P(\phi) \equiv \sum_{m=0}^{\infty} (a_m \cos m\phi + b_m \sin m\phi) \tag{9a}$$

$$Q(\phi) \equiv \sum_{m=0}^{\infty} (b_m \cos m\phi - a_m \sin m\phi) \tag{9b}$$

Cascade-Blade Spacing and Closure

To insure closure of the cascade blades, consider as depicted in Fig. 2 a closed contour C_0 about the unit circle that is

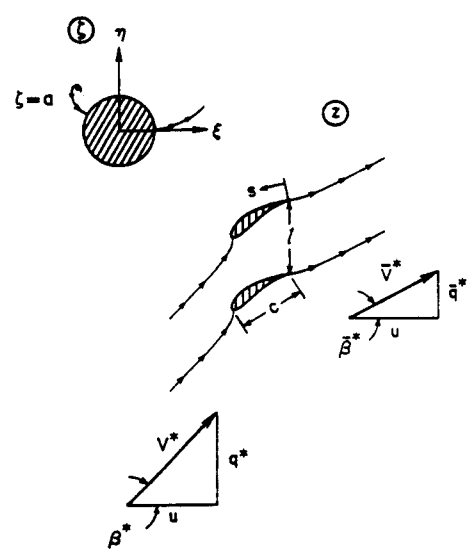

Fig. 1 Mapping from unit circle to the cascade.

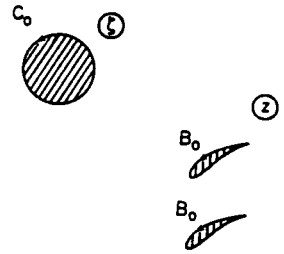

Fig. 2 Contour about the circle as mapped to the cascade.

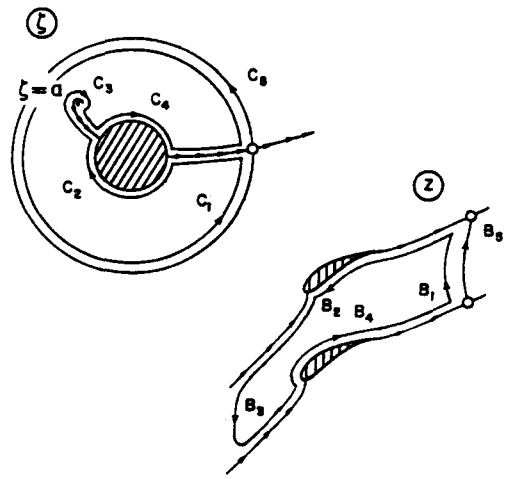

Fig. 3 Contours in the circle plane as mapped to the cascade plane.

mapped into a closed contour B_0 about each cascade blade. For any given cascade blade, it must be true that

$$\oint_{B_0} dz = \oint_{C_0} \frac{dz}{d\zeta} d\zeta = 0 \tag{10}$$

The contour $C_1 + C_2 + C_3 + C_4$ maps to $B_1 + B_2 + B_3 + B_4$ as shown in Fig. 3. Since no singularities are within the contour, the Cauchy-Goursat theorem gives

$$\int_{C_1} \frac{dz}{d\zeta} d\zeta + \int_{C_2} \frac{dz}{d\zeta} d\zeta + \int_{C_3} \frac{dz}{d\zeta} d\zeta + \int_{C_4} \frac{dz}{d\zeta} d\zeta = 0 \tag{11}$$

With $C_2 + C_4 = -C_0$, Eq. (11) becomes

$$\int_{C_1} \frac{dz}{d\zeta} d\zeta + \int_{C_3} \frac{dz}{d\zeta} d\zeta = 0 \tag{12}$$

In the limit that C_1 becomes C_5 and encloses the singularity at $\zeta = a$, the integral about C_5 becomes by the residue theorem

$$\oint_{C_5} \frac{dz}{d\zeta} d\zeta = 2\pi i \, \text{Res}(a) = \int_{B_5} dz = 1 \tag{13}$$

The last quantity $\int_{B_5} dz$ is simply the cascade spacing l used in Eq. (4). With $l = 2\pi i$, Eq. (13) gives

$$\text{Res}(a) = 1 \tag{14}$$

With this condition, substitution of Eq. (7) into Eq. (13) gives by the Cauchy integral formula

$$\text{Res}(a) = \left(1 - \frac{1}{a}\right)^{1-\varepsilon} \exp[f(a)] = 1 \tag{15}$$

Separation of Eq. (15) into the real and imaginary parts with $a = Ae^{i\alpha}$ yields

$$P(A, \alpha) = (1 - \varepsilon) \ln \left(\frac{A}{\sqrt{1 - 2A \cos \alpha + A^2}} \right) \tag{16a}$$

$$Q(A, \alpha) = -(1 - \varepsilon) \arg(A - e^{-i\alpha}) \tag{16b}$$

When these conditions are satisfied, the cascade blades will be closed, and the spacing will be $2\pi i$.

Cascade-Blade Coordinates

Cascade-blade coordinates are obtained by the integration of the mapping derivative about the unit circle to give

$$x(\phi) + iy(\phi) = -\int \frac{(2 \sin \phi/2)^{1-\varepsilon} \exp[P(\phi)]}{\sqrt{1 - 2A \cos(\alpha - \phi) + A^2}} \times \exp\{i[\phi/2 - \varepsilon(\pi/2 - \phi/2) - \arg(e^{i\phi} - Ae^{i\alpha}) + Q(\phi)]\} \, d\phi \tag{17}$$

Complex Potential Function

The flow outside the unit circle is characterized by two singularities: a vortex source at the point $\zeta = a$ and a vortex sink at the point $\zeta = \infty$. By use of the circle theorem, these singularities have reflections inside the circle, which when considered lead to the complex potential

$$F(\zeta) = Q[\ln(\zeta - a) + \ln(1 - \bar{a}\zeta) - \ln \zeta] - i\Gamma^*(\phi)[\ln(\zeta - a) + \ln(1 - \bar{a}\zeta)] - i\bar{\Gamma}^*(\phi) \ln \zeta \tag{18}$$

where Q is the source strength and $\bar{a}$ is the conjugate of a. At the present point in the development, the inlet and outlet circulation strengths $\Gamma^*(\phi)$ and $\bar{\Gamma}^*(\phi)$ may be thought of as constants. The notation $\bar{(\ )}$ is used to denote either a conjugate variable (e.g., $\bar{a}$), an outlet flow quantity [e.g., $\bar{\Gamma}^*(\phi)$], or as discussed later a cascade-blade lower-surface quantity.

Since the point $\zeta = 1$ is mapped to a sharp trailing edge, the Kutta condition requires that $\zeta = 1$ be a stagnation point. This condition gives

$$i\Gamma^*(\phi) = \frac{Q(a - \bar{a}) - i\bar{\Gamma}^*(\phi)(1 - a)(1 - \bar{a})}{1 - a\bar{a}} \tag{19}$$

In this case, the complex velocity becomes

$$\frac{dF}{d\zeta} = -\left(1 - \frac{1}{\zeta}\right) \frac{a[Q + i\bar{\Gamma}^*(\phi)] + \bar{a}[Q - i\bar{\Gamma}^*(\phi)]\zeta}{(\zeta - a)(1 - \bar{a}\zeta)} \tag{20}$$

Inlet and Outlet Conditions

The circulation strengths $\Gamma^*(\phi)$ and $\bar{\Gamma}^*(\phi)$ and the source strength Q are determined by considering the necessary inlet and outlet flows depicted in Fig. 1. The outlet flow is given by

$$\lim_{z \to \infty} \frac{dF}{dz} = u - i\bar{q}^*(\phi) = \lim_{\zeta \to \infty} \frac{dF/d\zeta}{dz/d\zeta} \tag{21}$$

In the limit, this becomes through the use of Eqs. (7) and (20)

$$u - i\bar{q}^*(\phi) = \frac{Q - i\bar{\Gamma}^*(\phi)}{\lim_{\zeta \to \infty} \exp[f(\zeta)]} \tag{22}$$

To relate the quantities u and $\bar{q}^*(\phi)$ to Q and $\bar{\Gamma}^*(\phi)$, another condition is placed on $f(\zeta)$, namely,

$$\lim_{\zeta \to \infty} \exp[f(\zeta)] = 1 \tag{23}$$

or

$$\lim_{r\to\infty} P(r, \phi) = 0 \tag{24a}$$

$$\lim_{r\to\infty} Q(r, \phi) = 0 \tag{24b}$$

It therefore follows that

$$Q = u, \qquad \Gamma^*(\phi) = \tilde{q}^*(\phi) \tag{25}$$

Proceeding in a similar manner, the inlet flow is given by

$$\lim_{z\to-\infty} \frac{dF}{dz} = u - iq^*(\phi) = \lim_{\zeta\to a} \frac{dF/d\zeta}{dz/d\zeta} \tag{26}$$

In the limit, this becomes

$$iq^*(\phi) = \frac{-u(a - \bar{a}) + i\bar{q}^*(\phi)(1 - a)(1 - \bar{a})}{1 - a\bar{a}} \tag{27}$$

In comparison with the Kutta condition, Eq. (19), it is necessary to have

$$\Gamma^*(\phi) = q^*(\phi) \tag{28}$$

Thus, the circulation and source strengths are now determined by the flow quantities in the cascade plane.

Equation (27) gives an important relation between the inlet and outlet flow angles. If it is taken that

$$\tan \beta^*(\phi) = \frac{q^*(\phi)}{u}, \qquad \tan \tilde{\beta}^*(\phi) = \frac{\tilde{q}^*(\phi)}{u} \tag{29}$$

Eq. (27) can be expressed as

$$2A \sin \alpha - (1 - A^2)\tan \beta^*(\phi) - (1 - 2A \cos \alpha + A^2)\tan \tilde{\beta}^*(\phi) = 0 \tag{30}$$

Consequently, once the vortex-source location $\zeta = a$ is selected, the specification of the inlet flow angle $\beta^*(\phi)$ sets the outlet flow angle $\tilde{\beta}^*(\phi)$ and vice versa.

Integral Constraints

Equations (16a), (16b), (24a), and (24b) are conditions on the mapping at the points $\zeta = a$ and $\zeta \to \infty$, respectively. These conditions at these points may be related to the mapping on the boundary of the unit circle. Specifically, for $\zeta \to \infty$, the Gauss mean value theorem applied exterior to the unit circle gives

$$\lim_{r\to\infty} P(r, \phi) = \frac{1}{2\pi}\int_0^{2\pi} P(\phi)\, d\phi = 0 \tag{31}$$

For $\zeta = a$, the Poisson integral formulas exterior to the unit circle yield

$$-P(A, \alpha) = \frac{1}{2\pi}\int_0^{2\pi} P(\phi) \frac{1 - A^2}{1 - 2A \cos(\alpha - \phi) + A^2}\, d\phi = -(1 - \varepsilon)/\pi \left(\frac{A}{\sqrt{1 - 2A \cos \alpha + A^2}}\right) \tag{32a}$$

$$-Q(A, \alpha) = \frac{1}{\pi}\int_0^{2\pi} P(\phi) \frac{A \sin(\alpha - \phi)}{1 - 2A \cos(\alpha - \phi) + A^2}\, d\phi = (1 - \varepsilon)\arg(A - e^{-i\alpha}) \tag{32b}$$

By Poisson's integral, $P(\phi)$ and $Q(\phi)$ are related as

$$Q(\phi) = \frac{1}{2\pi}\int_0^{2\pi} P(\psi)\cot \frac{\psi - \phi}{2}\, d\psi \tag{33}$$

Thus, if $P(\phi)$ is given, only Eqs. (31), (32a), and (32b) must be satisfied since $Q(\phi)$ may be determined from $P(\phi)$ through Eq. (38).

The three integral constraints, Eqs. (31), (32a), and (32b), involving $P(\phi)$ and three integral constraints involving $Q(\phi)$[22] are analogous in many ways to those integral constraints found for the isolated airfoil.[3] The essential difference is that for the cascade there are in a sense two freestreams: the inlet and outlet flows. For the isolated airfoil, only one condition in the form of an integral constraint must be satisfied to insure compatibility with the freestream flow. For the cascade, however, there are two conditions. First, there is the integral constraint, Eq. (31), on $P(\phi)$ to insure compatibility with the outlet flow. Second, the inlet flow condition leads to an algebraic condition, Eq. (30), relating the inlet and outlet angles. For the isolated airfoil, satisfaction of two integral constraints insures closure. Likewise, Eqs. (32a) and (32b) represent two integral constraints for closure of the cascade blades.

Relation Between the Mapping and the Complex Velocity

As yet, no reference has been made to the inverse design problem as classically posed by the specification of the velocity distribution. The necessary mapping conditions that insure closure and compatibility with the inlet and outlet flow have been presented. These special conditions may be satisfied by any number of mapping functions from which the cascade can be derived and the velocity distribution determined. Of course, the objective here is not to specify the mapping function per se. Rather, the goal is to specify the velocity distribution and from that derive the mapping, which then gives the cascade. With this in mind, the function $P(\phi)$ appearing in the integral constraints must be related to the complex velocity so that the velocity distribution may be explicitly involved in the integral constraints.

To this end, the complex velocity on the cascade blade is given by

$$\left.\frac{dF}{dz}\right|_{z=z_b} = \frac{dF/d\zeta|_{\zeta=\zeta_c}}{dz/d\zeta|_{\zeta=\zeta_c}} \tag{34}$$

where $z = z_b$ is on the cascade blade and $\zeta = \zeta_c$ is on the circle. In exponential form, the complex velocity on the cascade blade is expressed alternatively as

$$\left.\frac{dF}{dz}\right|_{z=z_b} = v^*(\phi)\exp[-i\theta^*(\phi)] \tag{35}$$

where $v^*(\phi)$ and $\theta^*(\phi)$ are, respectively, the design velocity distribution and flow angle about the cascade blade. On the circle, the complex velocity becomes

$$\left.\frac{dF}{d\zeta}\right|_{\zeta=\zeta_c} = \frac{2A\tilde{V}^*(\phi)|\cos[\alpha + \tilde{\beta}^*(\phi) - \phi/2]|\tau(\phi)}{1 - 2A \cos(\alpha - \phi) + A^2} \tag{36}$$

where

$$\tau(\phi) = (2 \sin \phi/2)\exp\{-i[\phi - \pi/2 - \pi^*(\phi)]\} \tag{37}$$

$$\tilde{V}^*(\phi) = \sqrt{u^2 + [\tilde{q}^*(\phi)]^2} \tag{38}$$

$$\pi^*(\phi) = \begin{cases} 0, & 0 \le \phi \le 2[\alpha + \tilde{\beta}^*(\phi)] - \pi \\ \pi, & 2[\alpha + \tilde{\beta}^*(\phi)] - \pi \le \phi \le 2\pi \end{cases} \tag{39}$$

Also, from Eq. (7), it is found that

$$\left.\frac{dz}{d\zeta}\right|_{\zeta=\zeta_c} = \frac{(2\sin\phi/2)^{1-\varepsilon}e^{P(\phi)}}{\sqrt{1-2A\cos(\alpha-\phi)+A^2}}\,\nu(\phi) \tag{40}$$

where

$$\nu(\phi) = \exp\{i[(1-\varepsilon)(\pi/2-\phi/2) - \arg(e^{i\phi}-a) + Q(\phi)]\} \tag{41}$$

When Eqs. (35), (36), and (40) are substituted into Eq. (34), it is found that

$$P(\phi) = -\mathcal{H}\left\{\frac{(2\sin\phi/2)^{-\varepsilon}\sqrt{1-2A\cos\alpha+A^2}\,v^*(\phi)}{2A\bar{V}^*(\phi)|\cos[\alpha+\bar{\beta}^*(\phi)-\phi/2]|}\right\} \tag{42a}$$

$$Q(\phi) = \theta^*(\phi) + \pi^*(\phi) - \phi/2 + \varepsilon(\pi/2-\phi/2) + \arg(e^{i\phi}-Ae^{i\alpha}) \tag{42b}$$

As desired, $P(\phi)$ is now related to $v^*(\phi)$.

Multipoint Design Capability of the Theory

In this section, it is discussed why $v^*(\phi)$ and $\bar{\beta}^*(\phi)$ are allowed to vary with ϕ. Figure 4 is used to aid in the discussion. The cascade blade is divided into a desired number of segments: five segments in Fig. 4. For this example, over the third segment ($\phi_2 \le \phi \le \phi_3$), the velocity distribution is prescribed as a constant v_3 for the outlet angle $\bar{\beta}_3$. For the fourth segment, the velocity distribution is prescribed as a constant v_4 for the outlet angle $\bar{\beta}_4$. The functions $v^*(\phi)$ and $\bar{\beta}^*(\phi)$ are made up of these piecewise functions defined by the values v_3, v_4, $\bar{\beta}_3$, and $\bar{\beta}_4$, respectively. At the junction ϕ_3 where $\bar{\beta}^*(\phi)$ jumps, $v^*(\phi)$ must also jump because $P(\phi)$ must remain continuous as discussed next.

Continuity Constraints

The requirement that $f(\zeta)$ be continuous on the boundary of the circle requires that $P(\phi)$ be continuous. In this case, at the junction between any two segments, it is required that

$$P_+(\phi_i) = P_-(\phi_i) \tag{43}$$

where the notations $(\,)_+$ and $(\,)_-$ are used to mean infinitesimally to the right and left of the point ϕ_i. Thus, for each junction on the cascade blade, a continuity condition arises to insure that for any given inlet or outlet angle the velocity distribution about the cascade blade is continuous.

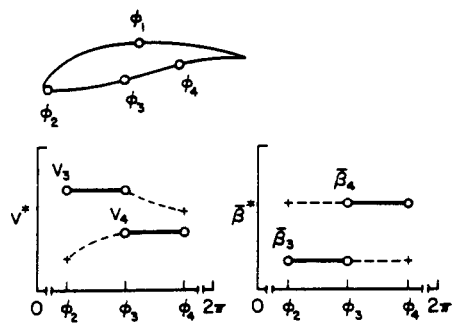

Fig. 4 Design velocity distribution and outlet flow angle distribution for the third and fourth cascade segments.

Leading- and Trailing-Edge Stagnation Point Conditions

By Eq. (42a), the design velocity distribution is expressed as

$$v^*(\phi) = \frac{2A\bar{V}^*(2\sin\phi/2)^{\varepsilon}|\cos[\alpha+\bar{\beta}^*(\phi)-\phi/2]|}{\sqrt{1-2A\cos\alpha+A^2}}\,e^{-P(\phi)} \tag{44}$$

As may be seen, stagnation points occur first at $\phi = 0$ and $\phi = 2\pi$ (i.e., the trailing edge), when $\varepsilon \neq 0$, and second at $\phi = \gamma \equiv 2[\alpha + \bar{\beta}^*(\phi)] - \pi$ (i.e., the aerodynamic leading edge). Consequently, the design velocity distribution at the trailing edge must vanish as

$$\lim_{\phi_+\to 0} v^*(\phi) \sim (\sin\phi/2)^{\varepsilon} g_+(\phi) \tag{45a}$$

$$\lim_{\phi_-\to 2\pi} v^*(\phi) \sim (\sin\phi/2)^{\varepsilon} g_-(\phi) \tag{45b}$$

whereas, at the aerodynamic leading edge γ, the velocity distribution must vanish as

$$\lim_{\phi_+\to\gamma} v^*(\phi) \sim |\cos[\alpha+\bar{\beta}^*(\phi)-\phi/2]|\,h_+(\phi) \tag{46a}$$

$$\lim_{\phi_-\to\gamma} v^*(\phi) \sim |\cos[\alpha+\bar{\beta}^*(\phi)-\phi/2]|\,h_-(\phi) \tag{46b}$$

and where $g_+(\phi)$, $g_-(\phi)$, $h_+(\phi)$, and $h_-(\phi)$ are positive, nonzero functions.

Basic Solution Formulation

It is helpful to identify the pertinent equations and outline the solution. From the onset, it should be mentioned that the specified quantities include 1) the design velocity distribution $v^*(\phi)$, 2) the design inlet and outlet flow angle distributions $\beta^*(\phi)$ and $\bar{\beta}^*(\phi)$, 3) the point $\zeta = a$, and 4) the trailing-edge parameter ε. These quantities must be specified such that 1) the flow angle relation, Eq. (30), is satisfied, 2) the stagnation point velocity laws, Eqs. (45a), (45b), (46a), and (46b), are not violated, 3) the continuity constraints, Eq. (43)—one coming from each junction—are satisfied, and 4) the integral constraints, Eqs. (31a), (32a), and (32b), on $P(\phi)$ are satisfied.

Clearly, to meet all of these restrictions, the specification of $v^*(\phi)$, $\beta^*(\phi)$, $\bar{\beta}^*(\phi)$, a, and ε cannot be entirely arbitrary. Thus, some degrees of freedom must be introduced into the specified parameters. Once this is done and all equations are satisfied, $P(\phi)$ is formed. From $P(\phi)$, the conjugate harmonic function $Q(\phi)$ is determined.[3] The functions $P(\phi)$ and $Q(\phi)$ together with a and ε are then used to find the cascade-blade coordinates through Eq. (17). Finally, for an arbitrary outlet angle $\bar{\beta}$ the velocity distribution $v(\phi)$ is determined through Eq. (44).

The remainder of this section is concerned with the solution of the governing equations and the introduction of the free parameters. First, the parameters a and ε are specified. Next, the design outlet flow angle distribution $\bar{\beta}^*(\phi)$ is specified piecewise as

$$\bar{\beta}^*(\phi) = \begin{cases} \bar{\beta}_1, & 0 \le \phi \le \phi_1 \\ \bar{\beta}_i, & \phi_{i-1} \le \phi \le \phi_i \quad i = 2, 3, \ldots, I-1 \\ \bar{\beta}_I, & \phi_{I-1} \le \phi \le 2\pi \end{cases} \tag{47}$$

where I is the total number of segments about the cascade blade. Based on the various specified $\bar{\beta}_i$ and a, the corresponding inlet flow angle for each segment is determined through application of the flow angle relation, Eq. (30). Alternatively, for any given segment, the inlet flow angle can be specified, from which the outlet flow angle is determined.

At this point, the design inlet and outlet flow angles are known for each segment of the cascade blade. Next, the design velocity distribution for each segment is specified in a similar piecewise manner as

$$v^*(\phi) = \begin{cases} v_1 w(\phi), & 0 \le \phi \le \phi_1 \\ v_i, & \phi_{i-1} \le \phi \le \phi_i \quad i = 2, 3, \ldots, I-1 \\ v_I \bar{w}(\phi), & \phi_{I-1} \le \phi \le 2\pi \end{cases} \tag{48}$$

The design velocity distribution for the first segment (and similarly for the last) is specified by the function $w(\phi)$ that is scaled by the constant v_1. For each intermediate segment ($i = 2, 3, \ldots, I-1$), the design velocity distribution is simply a constant v_i.

In specifying the design velocity distribution, the stagnation point velocity laws must not be violated. At the trailing edge, the design velocity distribution must therefore vanish as $(\sin \phi/2)^r$. Thus, $w(\phi)$ and $\bar{w}(\phi)$ must have as a factor $(\sin \phi/2)^r$. The function $w(\phi)$, termed the upper-surface recovery function, is defined as

$$w(\phi) = w_W^{\bar{\mu}}(\phi) w_S^{K_H}(\phi) w_F^{\epsilon}(\phi), \qquad 0 \le \phi \le \phi_1 \tag{49}$$

where

$$w_W(\phi) = 1 + K\left(\frac{\cos\phi - \cos\phi_W}{1 + \cos\phi_W}\right), \quad 0 \le \phi \le \phi_W \tag{50a}$$

$$w_S(\phi) = \begin{cases} 1 - 0.36\left(\dfrac{\cos\phi - \cos\phi_S}{1 - \cos\phi_S}\right)^2, & 0 \le \phi \le \phi_S \\ 1, & \phi_S \le \phi \le \phi_W \end{cases} \tag{50b}$$

$$w_F(\phi) = \begin{cases} \dfrac{\sin\phi/2}{\sin\phi_F/2}, & 0 \le \phi \le \phi_F \\ 1, & \phi_F \le \phi \le \phi_W \end{cases} \tag{50c}$$

where $\phi_W \equiv \phi_1$. The lower-surface recovery function $\bar{w}(\phi)$ is of the same form except that $w_W(\phi)$, $w_S(\phi)$, $w_F(\phi)$, and the parameters μ, K_H, K, ϕ_W, ϕ_S, and ϕ_F are replaced by $\bar{w}_W(\phi)$, $\bar{w}_S(\phi)$, $\bar{w}_F(\phi)$, $\bar{\mu}$, $\bar{K}_H$, $\bar{K}$, $\bar{\phi}_W \equiv \phi_{I-1}$, $\bar{\phi}_S$, and $\bar{\phi}_F$. The function $w_F^{\epsilon}(p)$ insures the proper behavior of the velocity distribution at the trailing edge. Briefly, the functions $w_W^{\bar{\mu}}(\phi)$ and $w_S^{K_H}(\phi)$ control to a great extent the main pressure recovery and the trailing-edge pressure recovery, respectively. Although these functions were developed for use in inverse airfoil design,[2] they are suitable for cascade design.

For each junction on the cascade blade, the continuity constraint must be satisfied. Satisfaction of this constraint for all junctions, excluding that at the trailing edge, gives

$$\frac{v_i}{\bar{V}_i|\cos(\alpha + \bar{\beta}_i - \phi_i/2)|} = \frac{v_{i+1}}{\bar{V}_{i+1}|\cos(\alpha + \bar{\beta}_{i+1} - \phi_i/2)|}$$
$$i = 1, 2, \ldots, I-1 \tag{51}$$

This recursion relation represents $I - 1$ equations for a cascade blade with I segments. The continuity equations serve to define the velocity levels v_i. This is done by specifying one of the I velocity levels. The remaining $I - 1$ velocity levels are determined by these $I - 1$ continuity equations.

The trailing-edge continuity constraint (applied at $\phi = 0$ and 2π) and the three integral constraints have yet to be satisfied. Substitution of $v^*(\phi)$ and $\bar{\beta}^*(\phi)$ into the integral constraints, Eqs. (31), (32a), and (32b), and the continuity Eq. (43) at the trailing edge leads to

$$a_{11}\mu + a_{12}\bar{\mu} + a_{13}K_H + a_{14}\bar{K}_H = b_1 \tag{52a}$$

$$a_{21}\mu + a_{22}\bar{\mu} + a_{23}K_H + a_{24}\bar{K}_H = b_2 \tag{52b}$$

$$a_{31}\mu + a_{32}\bar{\mu} + a_{33}K_H + a_{34}\bar{K}_H = b_3 \tag{52c}$$

$$a_{41}\mu + a_{42}\bar{\mu} + a_{43}K_H + a_{44}\bar{K}_H = b_4 \tag{52d}$$

Once the remaining recovery parameters (K, $\bar{K}$, ϕ_S, $\bar{\phi}_S$, ϕ_F, and $\bar{\phi}_F$) are specified, the coefficients a_{ij} and b_i are determined.[15] Afterwards, the system of Eqs. (52a–52d) is solved to give μ, $\bar{\mu}$, K_H, and $\bar{K}_H$. With the values of these last parameters determined, $P(\phi)$ is completely defined, after which $Q(\phi)$ is determined and the cascade-blade coordinates follow by integration of Eq. (17).

Newton Iteration

Specification of $v^*(\phi)$, $\beta^*(\phi)$, $\bar{\beta}^*(\phi)$, a, and ϵ and satisfaction of the basic equations do not lead automatically to a cascade with all of the desired characteristics, such as solidity and stagger. These latter quantities and others depend on the solution of the basic equations. Although some of the cascade design parameters are determined by the basic solution, many parameters are specified directly. These specified parameters include 1) a and ϵ, 2) the segment arc limits ϕ_i, 3) either the inlet or outlet flow angle, β_i or $\bar{\beta}_i$, for each segment, 4) one of the I velocity levels v_i, and 5) the recovery parameters K, $\bar{K}$, ϕ_S, $\bar{\phi}_S$, ϕ_F, and $\bar{\phi}_F$. Adjustment of each of these design parameters affects the solution of the basic equations and, as a result, the characteristics of the resulting cascade.

It is possible to take advantage of this fact to achieve the desired cascade characteristics. For instance, a change in the modulus of a, that is, the distance A to the vortex source, mainly affects the cascade solidity σ. Through Newton iteration, the sensitivity of σ to A can be numerically determined and used to find the change in A that leads to the desired σ. This process is not limited to a one-dimensional Newton iteration. Several of the cascade design parameters may be iterated to achieve cascade characteristics that are not otherwise directly specified.

Demonstration of the Method

In this section, four cascade designs are presented to illustrate the capability of the method. In each case the spacing is fixed to be 2π ($l = 2\pi i$), and the normal velocity is set to unity ($u = 1$). It should be mentioned that the examples presented are not intended for practical application since such would go beyond the scope of the present investigation.

For the first cascade, four segments are selected over which the following inlet angles of attack and arc limits are selected:

$$\beta_1 = \beta_2 = -15, \qquad \beta_3 = \beta_4 = -25 \text{ deg}$$
$$\phi_1 = 160, \qquad \phi_2 = 265.2, \qquad \phi_3 = 290 \text{ deg} \tag{53}$$

The trailing-edge parameter is taken as $\epsilon = 0$ so that the trailing edge ends in a cusp. The vortex-source location a is set by

$$A = 1.6, \qquad \alpha = 270 \text{ deg} \tag{54}$$

The flow-angle relation is used to find the outlet flow angles:

$$\bar{\beta}_1 = \bar{\beta}_2 = -45.46, \qquad \bar{\beta}_3 = \bar{\beta}_4 = -47.81 \text{ deg} \tag{55}$$

For $v_1 = 2.42$, the velocity levels are obtained from the continuity constraints and given by

$$v_2 = 2.42, \qquad v_3 = v_4 = 0.534 \tag{56}$$

Next, the recovery parameters are set as

$$K = \bar{K} = 1, \qquad \phi_S = 40, \qquad \bar{\phi}_S = 320 \text{ deg} \quad (57)$$

Since $\varepsilon = 0$, the parameters ϕ_F and $\bar{\phi}_F$ are not used. The coefficients in Eqs. (52a–52d) are determined and used to find

$$\mu = -0.00208, \quad \bar{\mu} = -6.19, \quad K_H = 6.91, \quad \bar{K}_H = 8.86 \quad (58)$$

With all of the design parameters defined, the cascade geometry is determined and shown in Fig. 5. Also shown in Fig. 5 and the others that follow are the circle and vortex source.

Even though all of the necessary mathematical conditions are satisfied by the cascade shown in Fig. 5, this alone does not always yield a practical cascade geometry. It is often desirable to specify K_H and $\bar{K}_H$ by Newton iteration so as to control the geometry of the profile in the vicinity of the trailing edge.[2-4] In particular, to improve the cascade shown in Fig. 5, the parameters K_H and $\bar{K}_H$ may be specified through Newton iteration on the design parameters ϕ_2 and v_1, i.e.,

$$\phi_2 \Rightarrow 0 = K_H - 0.5, \qquad v_1 \Rightarrow 0 = \bar{K}_H + 0.2 \quad (59)$$

where the notation "$\Rightarrow$" means that the design parameter has a first-order effect on the corresponding equation. Moreover, the solidity is specified to be $\sigma = 0.6$ by iteration of the parameter A, that is,

$$A \Rightarrow 0 = \sigma - 0.6 \quad (60)$$

Except for ϕ_2, v_1, and A (266.43 deg, 2.071, 1.246, respectively), which are determined by Newton iteration, the values from the first example are used. The resulting cascade geometry is shown in Fig. 6. As seen, the cascade is normal in appearance in that it is not bulbous or crossed. The corresponding velocity distributions are shown in Fig. 7 for the design inlet angles of -15 and -25 deg. To verify the method, these velocity distributions were compared with those predicted by a high-order panel method analysis,[23] and the agreement was excellent.[5]

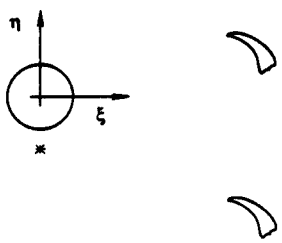

Fig. 5 Orientation of the unit circle with respect to the vortex source and resulting cascade geometry designed without Newton iteration.

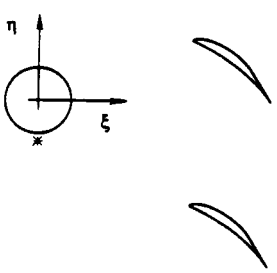

Fig. 6 Example cascade designed with Newton iteration for $K_H = 0.5$ and $\bar{K}_H = -0.2$.

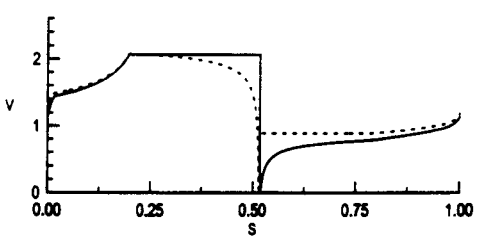

Fig. 7 Velocity distributions for $\beta = -15$ (solid line) and -25 deg (dotted line) for the cascade shown in Fig. 6.

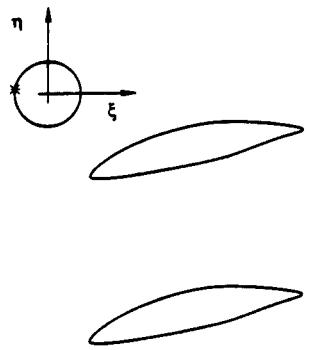

Fig. 8 Example cascade designed with Newton iteration for $K_H = 0.25$ and $\bar{K}_H = -0.25$.

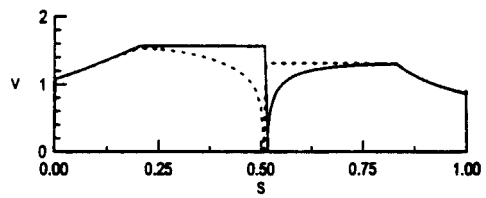

Fig. 9 Velocity distributions for $\beta = 4.55$ (solid line) and 4.45 deg (dotted line) for the cascade shown in Fig. 8.

The next example illustrates a four-segment cascade designed to have a rounded trailing edge ($\varepsilon = 1$) and desired segment velocity distributions for specified outlet angles. The rear stagnation point in the present method is not determined with respect to viscous considerations; rather, it is set at the point $\zeta = 1$ in accordance with the mapping. The following parameters are specified:

$$\bar{\beta}_1 = \bar{\beta}_2 = 4.55, \quad \bar{\beta}_3 = \bar{\beta}_4 = 4.45 \text{ deg}$$
$$\varepsilon = 1, \quad A = 1.01, \quad \alpha = 171.25 \text{ deg}, \quad K = \bar{K} = 1$$
$$\phi_S = 25, \quad \bar{\phi}_S = 335, \quad \phi_F = 15, \quad \bar{\phi}_F = 345 \text{ deg} \quad (61)$$

Newton iteration is used to control the trailing-edge closure parameters as

$$\phi_2 \Rightarrow 0 = K_H - 0.25, \qquad v_1 \Rightarrow 0 = \bar{K}_H + 0.25 \quad (62)$$

The corresponding geometry and velocity distribution at the outlet design angles of attack are shown in Figs. 8 and 9, respectively. A blunter trailing edge could be achieved by specifying larger values for K_H and $\bar{K}_H$.

The last example is for a cascade blade with five segments. The following parameters are specified:

$$\beta_1 = \beta_2 = 65, \quad \beta_3 = 70, \quad \beta_4 = \beta_5 = 60 \text{ deg}$$
$$\varepsilon = 1/18, \quad A = 1.1, \quad \alpha = 105 \text{ deg}, \quad K = \bar{K} = 1$$
$$\phi_S = 40, \quad \bar{\phi}_S = 330, \quad \phi_F = 20, \quad \bar{\phi}_F = 345 \text{ deg} \quad (63)$$

Newton iteration is used to determine ϕ_1, ϕ_2, ϕ_3, ϕ_4, and v_1 so that

$$\phi_1 \Rightarrow 0 = x_1/c - 0.65, \qquad \phi_2 \Rightarrow 0 = x_2/c - 0.1$$
$$\phi_3 \Rightarrow 0 = K_H - 0.8, \qquad \phi_4 \Rightarrow = 0 = x_4/c - 0.5$$
$$v_1 \Rightarrow 0 = \bar{K}_H + 0.3 \quad (64)$$

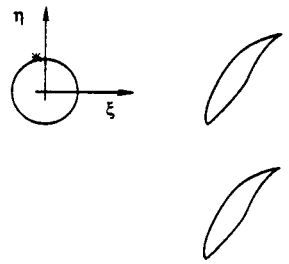

Fig. 10 Example cascade designed with Newton iteration for K_H = 0.8, $\bar{K}_H$ = −0.3, x_1/c = 0.65, x_2/c = 0.1, and x_4/c = 0.5.

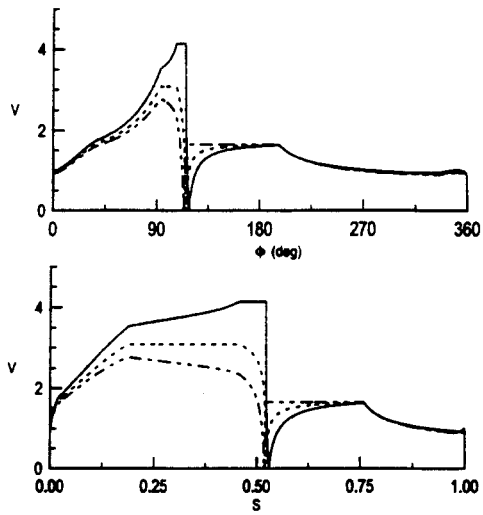

Fig. 11 Velocity distribution plotted as a function of ϕ and s for β = 60 (dot-dash line), 65 (dotted line), and 70 deg (solid line) for the cascade shown in Fig. 10.

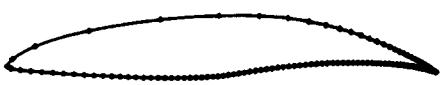

Fig. 12 Cascade blade of Fig. 10 with symbols plotted at each of the 120 points to illustrate point spacing.

The arc limits ϕ_1, ϕ_2, and ϕ_4 are determined so that these points map to a specified chordwise location. The cascade geometry is shown in Fig. 10. Figure 11 shows the velocity distributions as a function of ϕ and s/c for the design inlet angles of 60, 65, and 70 deg.

This cascade illustrates a limitation of the method. By the transformation, the cascade spacing is fixed as $2\pi i$. The solidity can be changed only by changing the cascade-blade chord. Because the vortex source is mapped infinitely far upstream of the cascade, points very near the vortex source tend to be mapped far upstream. Thus, as the vortex source moves closer to the circle, the part of the circle nearest the vortex source stretches upstream in the cascade plane; that is, the cascade-blade chord increases, which, in turn, increases the solidity. When an attempt is made to increase the chord much beyond 2π (i.e., increase the solidity much beyond unity), the stretching becomes extreme near the cascade-blade leading edge. In this case, numerical integration of the mapping derivative [Eq. (17)] for the coordinates leads to inaccuracies. For example, Fig. 12 shows the cascade blade as determined by using 120 equidistant points about the circle. As seen, the stretching is significant but, in this case, not significant enough to introduce inaccuracies into the blade coordinates. As suggested by Sanz,[24] mapping the circle onto an ellipse would mitigate such difficulties in designing high-solidity cascades.

Conclusions

This work demonstrates the intrinsic advantage of the use of conformal mapping in inverse cascade design, namely, its ability to allow for multipoint design. As shown by the first example cascade, however, this alone does not make the use of conformal mapping practical. The basic solution of the inverse problem can readily lead to unrealistic cascade profile shapes, i.e., bulbous or crossed profiles. This difficulty and others discussed collectively account for the diminishing use of conformal mapping in cascade design. The current approach, however, overcomes these problems by basing the numerical solution formulation on a successful procedure developed for inverse airfoil design. In particular, Newton iteration is used to adjust some design parameters (which are otherwise directly specified) so as to obtain the desired cascade characteristics (which are otherwise determined as part of the solution). Through this technique, characteristics such as the cascade solidity and stagger and the cascade-blade velocity distribution may be directly controlled. As a result, practical multipoint inverse cascade design is now possible.

Acknowledgments

This work was sponsored by the NASA Langley Research Center under Grant NGT-50341. The author expresses his appreciation to Mark Maughmer of the Pennsylvania State University for his helpful discussions and Richard Eppler of Universität Stuttgart for his comments related to this work and to the verification of the method.

References

[1]Gostelow, J. P., *Cascade Aerodynamics*, Pergamon Press, Oxford, England, UK, 1984.

[2]Eppler, R., *Airfoil Design and Data*, Springer-Verlag, New York, 1990.

[3]Selig, M. S., and Maughmer, M. D., "Multipoint Inverse Airfoil Design Method Based on Conformal Mapping," *AIAA Journal*, Vol. 30, No. 5, 1992, pp. 1162–1170.

[4]Selig, M. S., and Maughmer, M. D., "Generalized Multipoint Inverse Airfoil Design," *AIAA Journal*, Vol. 30, No. 11, 1992, pp. 2618–2625.

[5]Selig, M. S., "Multi-Point Inverse Design of Isolated Airfoils and Airfoils in Cascade in Incompressible Flow," Ph.D. Thesis, Dept. of Aerospace Engineering, Pennsylvania State Univ., University Park, PA, May 1992.

[6]Mangler, W., "Die Berechnung eines Tragflügelprofiles mit vorgeschriebener Druckverteilung," *Jahrbuch der Deutschen Luftfahrtforschung*, Vol. 1, 1938, pp. 46–53; English translation, Air Ministry of London, Translation 932, 1940.

[7]Lighthill, M. J., "A New Method of Two-Dimensional Aerodynamic Design," Aeronautical Research Council, R&M 2112, England, UK, April 1945.

[8]Garrick, I. E., "Conformal Mapping in Aerodynamics, with Emphasis on the Method of Successive Conjugates," *National Bureau of Standards Applied Mathematics Series 18: Constructions and Application of Conformal Maps*, Washington, DC, 1952, pp. 137–147.

[9]Abbott, I. H., "Airfoils: Significance and Early Development," *The Evolution of Aircraft Wing Design*, AIAA Symposium, AIAA, New York, 1980, pp. 23, 24.

[10]Lighthill, M. J., "A Mathematical Method of Cascade Design," Aeronautical Research Council, R&M 2104, England, UK, June 1945.

[11]Elizarov, A. M., Il'inskiy, N. B., and Potashev, A. V., "Aerodynamic Airfoils Design by Quasi-Solutions Method in Inverse Boundary-Value Problems," *Advances in Mechanics*, Vol. 4, No. 2, 1991, pp. 49–91.

[12]Wilkinson, D. H., "Analysis and Design of Aerofoils and Cascades in Incompressible Flow," *Journal of Science and Technology*, Vol. 36, No. 2, 1969, pp. 99–104.

[13]Schwering, W., "Design of Cascades for Incompressible Plane Potential Flows with Prescribed Velocity Distribution," American Society of Mechanical Engineers, ASME Paper 70-GT-87, 1970.

[14]Lewis, R. I., "A Method for Inverse Aerofoil and Cascade Design by Surface Vorticity," American Society of Mechanical Engineers, ASME Paper 82-GT-154, 1982.

[15]Costello, G. R., "Method of Designing Cascade Blades with Prescribed Velocity Distributions in Compressible Potential Flows," NACA Rept. 978, 1950.

[16]Costello, G. R., Cummings, R. L., and Sinnette, J. T., Jr., "Detailed Computational Procedure for Design of Cascade Blades with

Prescribed Velocity Distributions in Compressible Potential Flows," NACA Rept. 1060, 1952.

[17]Papailiou, K., "Blade Optimization Based on Boundary Layer Concepts," von Kármán Inst. for Fluid Dynamics, Course Note 60, Rhode-Saint-Genese, Belgium, March 1967.

[18]Ruzicka, M., and Spacek, L., "A Mathematical Method for Design of Turbine Blade Cascades for Small Subsonic Mach Numbers," National Research Inst. for Machine Design, Monographs and Memoranda, No. 29, Bechovice, 1981.

[19]Rosenblatt, S., and Woods, L. C., "A Method of Cascade Design for Two-Dimensional Incompressible Flow," Aust. Aeronautical Research Committee, Rept. ACA-58, March 1956.

[20]Garrick, I. E., "On the Plane Potential Flow Past a Lattice of Arbitrary Airfoils," NACA Rept. 788, 1944.

[21]Howell, A. R., "A Theory of Arbitrary Aerofoils in Cascade," *Philosophical Magazine*, Vol. 39, No. 299, 1948, pp. 913–927.

[22]Selig, M. S., "Multi-Point Inverse Design of an Infinite Cascade of Airfoils," AIAA Paper 92-2650, June 1992.

[23]Eppler, R., "Airfoils Program System User's Guide," Institut A für Mechanik, Universität Stuttgart, Stuttgart, Germany, March 1991.

[24]Sanz, M. J., "Design of Supercritical Cascades with High Solidity," *AIAA Journal*, Vol. 21, No. 9, 1983, pp. 1289–1293.